

Comprehensive Optical, Morphological, and Antibacterial Analysis of Gold Nanoparticles Synthesized Using Aqueous Extract of *Plumeria pudica* Leaves

Kumari Anamika¹ , Manoranjan Behera^{1,*} , Anshuman Sarangi² 

¹ Silicon University, Odisha, India; kumari.anamika@silicon.ac.in(K.A.); manoranjan@silicon.ac.in (M.B.);

² Trident Academy of Creative Technology, Odisha, India; anshumanbbsr2@gmail.com;

* Correspondence: manoranjan@silicon.ac.in (M.B.);

Scopus Author ID 7004588847

Received: 29.07.2024; Accepted: 6.10.2024; Published: 14.02.2025

Abstract: This article reports on the bio-synthesis and inclusive characterization of gold nanoparticles (Au NPs) using an aqueous extract of *Plumeria pudica* leaves. An increase in the Au content in the nanofluids causes a bathochromic shift in the $\pi \rightarrow \pi^*$ band at 324 nm of the phytochemical. This redshift occurs because the dielectric constant of the nanofluid medium changes as the number of stabilizing molecules per gold nanoparticle decreases. Gold NPs induced a minor shift in some of the vibrational bands and a slight improvement in band intensity, suggesting the existence of a weak interaction between the nanoparticles and plant molecules. The redshift accompanied by quenching in the photoluminescence intensity of the $\pi^* \rightarrow \pi$ light emission band at 414 nm further corroborates a donor-acceptor interaction between the nanoparticles and plant molecules. A linear Stern-Volmer plot with a Stern-Volmer constant of $7.72 \times 10^3 \text{M}^{-1}$ suggests a dynamic quenching mechanism. The position of Bragg's diffraction plane and the application of the extinction rule to the X-ray diffraction pattern predicts a face-centered cubic lattice for the synthesized Au NPs. Gold NPs are nearly spherical, and their cluster size increases with Au content, as observed in scanning and transmission electron micrographs. Dynamic light scattering experiments indicate an average hydrodynamic diameter between 140-170 nm and a negative surface charge on the gold nanoparticles. The synthesized gold nanofluids in an aqueous solvent show a little antibacterial effect against three microorganisms: *Bacillus subtilis*, *Pseudomonas aeruginosa*, and *Escherichia coli* with respect to a standard macrolide antibiotic.

Keywords: *Plumeria pudica*; nanofluids; redshift; light quenching; stern-volmer plot; hydrodynamic diameter; zeta-potential; microorganisms.

© 2025 by the authors. This article is an open-access article distributed under the terms and conditions of the Creative Commons Attribution (CC BY) license (<https://creativecommons.org/licenses/by/4.0/>).

1. Introduction

The bio-reduction method, a bottom-up approach, is widely used today to synthesize nanomaterials (NMs) due to its cost-effectiveness, simplicity, medicinal efficacy, reduced toxicity, and environmental friendliness. Various metallic nanoparticles (NPs) such as gold (Au), silver (Ag), nickel (Ni), copper (Cu), iron (Fe), and manganese (Mn) have been synthesized using phytochemicals for a range of applications, including bio-medicals, sensing, solar cells, heat transfer, and photocatalysis [1-3]. Biosynthesized Au-NPs have been proven to act as anticancer, antimicrobial, antidiabetic, antiplatelet, antiviral, antioxidant, and anti-inflammatory agents [2-5]. In the plant-mediated biosynthesis of NMs, plant parts such as leaves, bark, stems, flowers, and roots are used as raw materials. These parts are first washed

in water, then cut into small pieces and boiled in double-distilled water to obtain the aqueous extract for the synthesis of NMs. The plant-mediated method outweighs the microorganism route because it does not require the extensive care needed to maintain a microbial culture [6-8]. In biosynthesis, factors such as the concentration of plant extract and precursor salt, the nature of the stabilizing agent, pH, temperature, stirring rate, and stirring time play a crucial role in developing NMs of specific shapes and sizes [9]. Phytochemicals such as polyphenols, flavonoids, quinic acids, terpenes, thiophenes, saponin, sterols, and quercetin not only act as reducing agents to convert metal ions to their atomic state but also help prevent the formation of large particle clusters [5-7].

Fruit extracts from *Aegle marmelos*, *Eugenia jambolana*, and *soursop* were employed in the green synthesis of Au-NPs, which were effective against the MCF-7 breast cancer cell line [1]. The report suggests that the in-vitro anticancer activity of *soursop*-stabilized AuNPs at a concentration of $98 \pm 4 \mu\text{g}$ per mL outperformed those stabilized with *Aegle marmelos* and *Eugenia jambolana*. Leaf extract of the *Mentha longifolia* plant was used to synthesize Au-NPs to evaluate their anti-breast cancer efficacy. These Au-NPs demonstrated effective anti-breast cancer effects against breast adenocarcinoma, breast carcinoma, breast infiltrating ductal cell carcinoma, and breast infiltrating lobular carcinoma cell lines without exhibiting cytotoxicity against normal cell lines [2]. Muniyappa *et al.* [3] reported that *Curcuma pseudomontana* isolated curcumin-stabilized Au-NPs exhibit excellent antibacterial activity against *Pseudomonas aeruginosa*, *Staphylococcus aureus*, *Bacillus subtilis*, and *Escherichia coli*. Additionally, these Au-NPs demonstrate significant antioxidant and radical scavenging activities. The phenolic ($-\text{OH}$) exhibited at 3410 cm^{-1} and carbonyl ($-\text{CO}$) groups at 1635 cm^{-1} are responsible for the formation and stabilization of curcumin-coated Au-NPs. Grape extract-mediated synthesis of gold nanoparticles exhibited significant antibacterial activity against *E. coli* and *B. subtilis* and antifungal effects against the yeast *Candida albicans* [4]. Various chemicals in the grape extract, such as gallic acid, catechin, caffeic acid, and cyanidin-3-O-glucoside, reduce Au^{3+} ions to $\text{Au}(0)$ and stabilize the nanoclusters. The lone pairs of electrons on the oxygen atoms of these chemicals provide electrons to Au^{3+} ions for the bio-reduction process.

Au-NPs synthesized using aqueous *Chrysothemispulchella* leaf extracts exhibited anticancer and antimicrobial activities. Ogwuche *et al.* [5] reported that the strength and usefulness of these Au-NPs against pathogens such as Methicillin-resistant *Staphylococcus aureus*, *Escherichia coli*, and *Candida albicans* increase with higher nanoparticle concentrations. Matteis *et al.* [6] synthesized AuNPs capped with polyphenols present in the extract of the leaves of the *Laurus nobilis*, where the hydroxyl ($-\text{OH}$) groups facilitated the development of a negatively charged surface. This was confirmed through zeta potential measurements with a value of -34 mV . The involvement of hydroxyl ($-\text{OH}$) groups in forming Au-NPs as both reducing and capping agents was studied using FTIR spectroscopy [7]. A shift to lower wavenumbers in various vibrational bands, such as C-H, C-N, and C=O stretching bands of plant phytochemicals, suggested an interaction between the NPs and the molecules of the plant extract.

The antibacterial effects of Au-NPs synthesized using grape extract were studied on Gram-positive and Gram-negative microorganisms [8]. The findings suggested that the antibacterial action may primarily result from the cellular processes and physical interactions between the nanoparticles and the bacteria. The distribution of Au-NPs was studied using dynamic light scattering (DLS). A zeta potential value of -14.8 mV indicates the formation of

a negatively charged surface on the nanoparticles, which is responsible for the excellent colloidal stability exhibited by the nanofluids [10]. Ogwuche *et al.* [11] investigated the antibacterial and anticancer properties of gold nanoparticles synthesized using *Chrysothemispulchella* leaf extract. They dissolved the Au NPs in a non-aqueous solvent and reported a minimum inhibitory concentration of 50 $\mu\text{g/mL}$ against most clinical pathogenic microbes. From their dynamic light scattering study, Bidan *et al.* [12] reported a hydrodynamic diameter of 140 nm and a polydispersity index 0.496 for Au NPs synthesized using Jasminum Sambac leaf extract. They suggested that phytochemicals in the plant extract interact with Au NPs via oxygen atoms and that the surface of the Au NPs has a zeta potential of -9.37 mV.

In this article, we report the synthesis of Au-NPs using *Plumeria pudica* leaf extracts in an aqueous medium and its mild antibacterial activity against specific microorganisms. To our knowledge, this is the first report on the aqueous-mediated synthesis of Au-NPs using *Plumeria pudica* leaf extract.

2. Materials and Methods

2.1. Chemicals.

Ultrapure gold chloride hydrate (Tetrachloroauric acid, $\text{HAuCl}_4 \cdot x\text{H}_2\text{O}$) with a purity of 99.99% and approximately 49% gold content was purchased from SRL Pvt. Ltd., India. It was utilized to create a highly diluted gold solution in deionized water without additional purification.

Preparation of plant extract.

Leaves of the *Plumeria Pudica* plant were collected from our university campus and thoroughly washed with double-distilled water. After drying at room temperature, the leaves were chopped into pieces. Twenty grams of the chopped leaves were placed in a beaker with 200 mL of deionized water and heated on a magnetic stirrer hot plate at 105°C for 2 hours. The resulting aqueous extract was then filtered to obtain a clear yellowish-green solution, which was preserved in a refrigerator to synthesize Au-NPs.

2.3. Biosynthesis of Au-NPs.

Gold nanoparticles were synthesized using a bio-reduction method by adding 0.5 mL, 1.0 mL, 1.5 mL, 2.0 mL, and 2.5 mL of 1 mM HAuCl_4 solution to five separate 50 mL beakers, each containing 5 mL of aqueous plant extract. Figure 1 shows photographs of five nanofluids prepared for characterization. The mixture was then heated on a magnetic stirrer at 50°C and stirred for 20 minutes. The color change from yellowish to bluish-black indicated the formation of Au-NPs in the extract solution. Following this procedure, five nanofluids with different concentrations of Au-NPs were prepared and preserved in a refrigerator for characterization.



Figure 1. Au Nanofluids with (a) 0; (b) 4.32; (c) 7.2; (d) 10/08; (e) 14.4; (f) 18.72 mM Au NPs.

2.4. Characterization techniques.

Phytochemical-capped Au-NPs were characterized using various instrumental techniques, including UV–visible spectroscopy, transmission electron microscopy (TEM), X-ray diffraction (XRD), Fourier transform infrared (FT-IR) spectroscopy, photoluminescence (PL) spectroscopy, field-emission scanning electron microscopy (FE-SEM), and zeta-sizer analysis. UV-vis spectroscopy (200–1000 nm) was employed to detect the surface plasmon resonance (SPR) band of Au-NPs in the nanofluids. FT-IR analysis, conducted in the wavenumber range of 4000-400 cm^{-1} , studied the interaction between the nanoparticles and phytochemicals present in the plant extract. A Perkin–Elmer (Model LS 55) luminescence spectrometer was used to obtain the emission spectra of the plant extract and the synthesized Au nanofluids. TEM images were obtained using a Hitachi HT-7700 microscope to examine the shape, size, and distribution of the crystalline Au-NPs. The lattice type and crystallite size were determined from the XRD pattern obtained with a Panalytical X’Pert3 diffractometer. The hydrodynamic diameter and zeta potential were measured using a Malvern Zeta-sizer. The antibacterial activity was assessed using the agar well diffusion method, and the zone of inhibition was measured to evaluate the antibacterial efficacy of the prepared Au nanofluids.

3. Results and Discussion

3.1. UV-visible absorption spectra of Au-nanofluids.

The synthesized Au nanofluids in an aqueous medium were characterized using a UV-visible spectrophotometer in the 200-800 nm wavelength range. Figure 2A shows the absorption spectra of phytochemical-stabilized Au nanofluids containing (b) 4.32 mM, (c) 7.2 mM, (d) 10.08 mM, (e) 14.4 mM, and (f) 18.72 mM Au-NPs. The position of the Surface Plasmon Resonance (SPR) band in an absorption spectrum for a nanofluid depends on factors such as shape, size, dielectric constant of the medium, nature of the stabilizing agent, and aggregation [1-3].

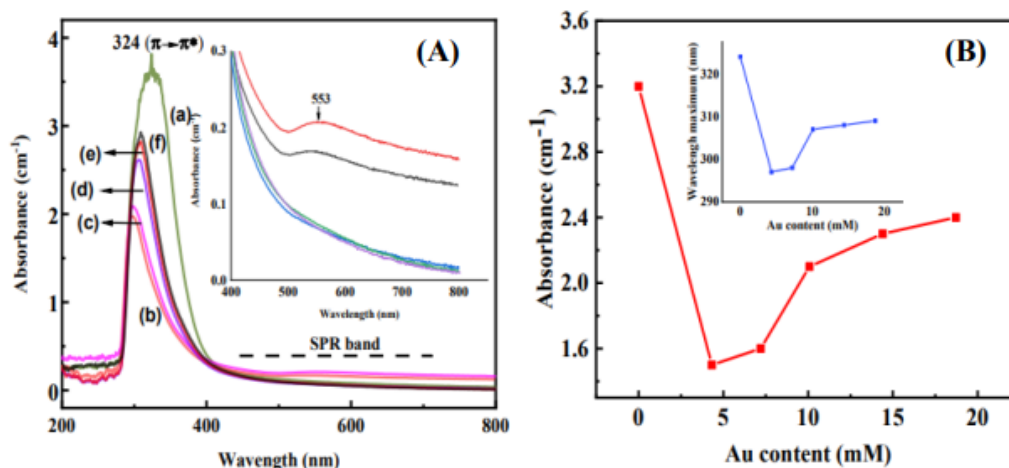


Figure 2.(A) Absorption spectra of Au Nanofluids with (a) 0, (b) 4.32; (c) 7.2; (d) 10.08; (e) 14.4; and (f) 18.72 mM Au NPs (*insert shows the SPR band of Au NPs*);(B) Variation of absorbance with Au content (*insert shows variation of wavelength maximum against Au content*).

A characteristic broad band centered at 553 nm (see the insert) is attributed to the SPR band of spherically shaped Au-NPs [1-3]. Figure 2A (a) shows the absorption spectrum for the plant extract, which exhibits a band at 324 nm. Muniyappan *et al.* [3] reported a broad band at

437 nm for *Curcuma pseudomontana* plant extract and an SPR band at 542 nm for the Au NPs. This band is attributed to the $\pi \rightarrow \pi^*$ electronic transition from the unsaturated part of the phytochemicals present in the plant extract [2]. Figure 2B shows that the absorbance of the $\pi \rightarrow \pi^*$ electronic transition decreases from 3.2 for the plant extract to 1.5 for sample (b), which contains 4.72 mM of Au NPs. Reduction in the absorbance value is due to the donor-acceptor type interaction between solute particles and solvent molecules.

Additionally, as the Au content increases, the absorbance rises from 1.5 for sample (b) to 2.4 for sample (f), which contains 18.72 mM of Au NPs. This variation in absorbance with the concentration of Au NPs is consistent with the Beer-Lambert law of light absorption. The absorption spectrum demonstrates a bathochromic shift in the $\pi \rightarrow \pi^*$ (from b to e) with increased Au content in the nanofluids. A similar variation was observed (see insert in Figure 2B) between the wavelength maximum (λ_{max}) and the concentration of Au NPs. The shift of the band towards longer wavelengths with an enhancement in the absorbance value suggests an increase in the size of the nanoparticles [1]. This occurs because, as the Au content increases, the number of stabilizing molecules per gold nanoparticle decreases, leading to a change in the dielectric constant of the nanofluid medium[13].

3.2. FTIR spectra.

Vibrational spectra were analyzed to study possible interactions between NPs and molecules present in the plant extract and to gain an idea of the interaction site of the molecule. The plant extract from the Plumeria family contains phytochemicals with functional groups such as $-\text{OH}$, $-\text{C}=\text{O}$, and $-\text{COOH}$ [14]. Figure 3 shows the vibrational spectra of phytochemical-stabilized Au Nanofluids with (a) 0, (b) 4.32, (c) 7.2, (d) 10.08; (e) 14.4, and (f) 18.72 mM Au NPs. In Figure 3, plot (a) shows the vibrational spectrum for the plant extract without any Au-NPs. The vibrational spectrum of the plant extract, both with and without Au NPs in an aqueous medium, appears similar at first glance. However, slight shifts in the band positions and changes in the intensity of some specific bands can be observed upon closer inspection. The spectra show peaks at 647 cm^{-1} , 1456 cm^{-1} , 1636 cm^{-1} , and 3331 cm^{-1} , corresponding to CH_2 in-plane rocking, CH_2 in-plane scissoring, $\text{C}=\text{O}$ stretching, and OH stretching vibrations, respectively [3].

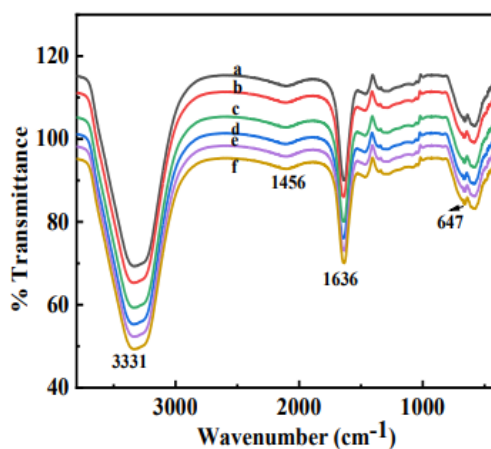


Figure 3. FTIR spectra of Au Nanofluids with (a) 0, (b) 4.32; (c) 7.2; (d) 10.08; (e) 14.4; and (f) 18.72 mM Au NPs.

Figure 4 shows a minor shift in band position and slight enhancement in band intensity upon the inclusion of Au-NPs in the plant extract, suggesting a weak interaction (Au-O bond)

between the nanoparticles and plant molecules [12]Tripathy *et al.* [15] reported similar findings to those presented in this article. Our results also indicate that the plant molecules interact with the nanoparticles via carbonyl and alcohol functional groups, as evidenced by an increase in band intensity and a shift of the band positions towards lower wavenumbers (see Figure 4).

The red shift of the vibrational band, as shown in Figure 4 is due to a decrease in the number of plant molecules relative to the Au nanoparticles (NPs) as the concentration of Au NPs in the nanofluids increases.

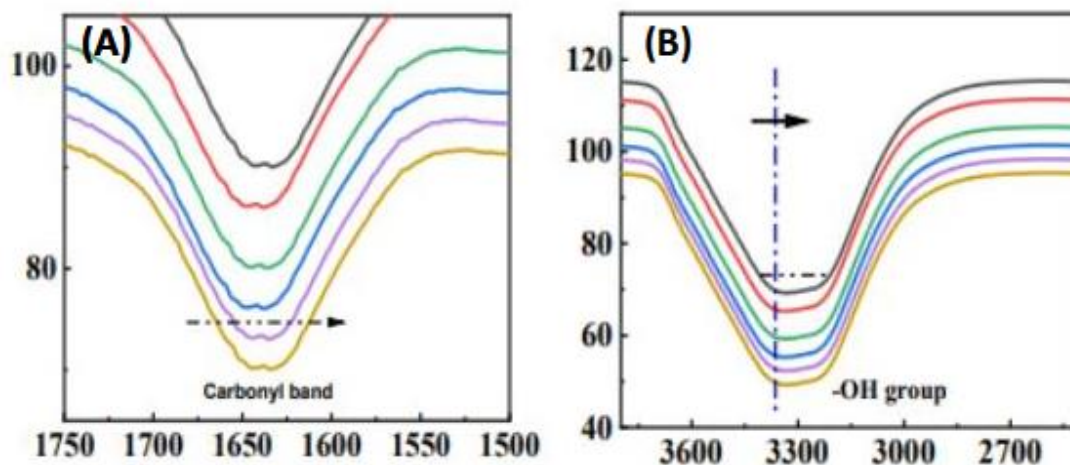


Figure 4. Vibrational band: (A)carbonyl band;(B)hydroxyl band of plant molecules.

The non-bonding electrons in these groups participate in the bio-reduction process to convert Au^{3+} -ions to zero-valent Au-atom. Rosyidah *et al.* [7] reported that some functional groups of the phytochemicals in the plant extract act as both reducing and capping agents. In their report on the optical study of *Mimusopselengi* raw fruit extract-mediated synthesis of gold nanoparticles (Au NPs), Tripathy *et al.* [15] also suggested that the oxygen atoms in quercetin molecules are responsible for both the reduction and stabilization of the nanoparticles.

3.3. PL spectra.

Figure 5 shows the emission spectra of the plant extract in an aqueous medium and Au nanofluids with varying amounts of Au nanoparticles. The emission spectrum of the plant extract without Au-NPs exhibits a broad peak (λ_{max}) at 414 nm, attributed to the $\pi^* \rightarrow \pi$ electronic transition. Behera and Ram [16] reported a broad peak at 392 nm for the carbonyl group in the poly(vinyl pyrrolidone) polymer. When 50 mM of Au nanoparticles are added to the plant extract, the λ_{max} shifts to 423 nm, indicating a 10 nm redshift (see insert of Figure 5). This band shift suggests an interaction between the active regions of the plant molecules and the Au NPs.

Furthermore, the plot shows that with 200 mM of Au NPs in the plant extract, the λ_{max} increases to 441 nm. The light emission intensity of the plant molecules has decreased by 70% with the presence of 200 mM of Au nanoparticles. This significant reduction in PL intensity suggests a donor-acceptor interaction between the plant molecules and Au nanoparticles, where the plant molecules act as electron donors. A similar result has already been suggested for polymer-capped Au NPs in an aqueous medium [16].

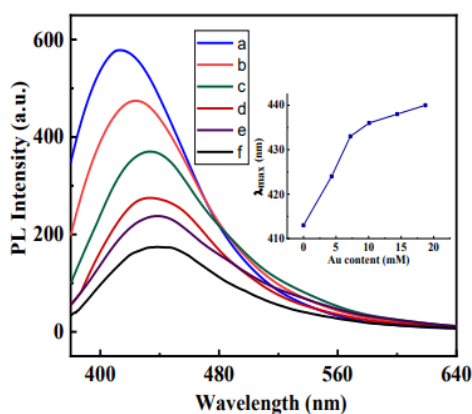


Figure 5. Emission spectra of Au Nanofluids with (a) 0, (b) 4.32; (c) 7.2; (d) 10.08; (e) 14.4; and (f) 18.72 mM Au NPs (*insert shows the variation of emission band position with Au content*)

We investigated the quenching of emission light intensity by plotting PL intensity against Au content (Figure 6) and discovered a non-linear variation with Au content. This finding further indicates a donor-acceptor-type interaction between molecules.

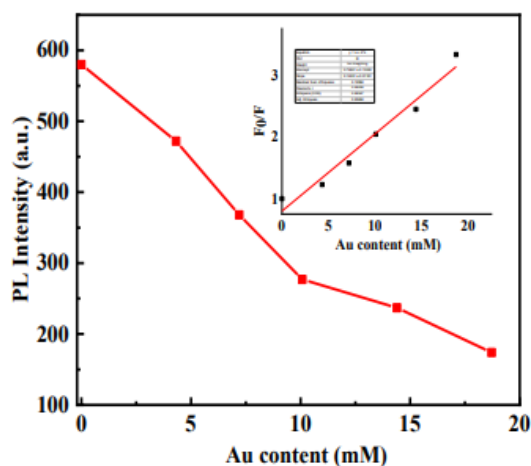


Figure 6. Variation of PL intensity with Au content (*insert shows the Stern-Volmer plot*).

To determine the quenching mechanism in our samples, we analyzed the Stern-Volmer plot using the standard equation: $F_0/F=1+ K_{SV} [Q]$, where F_0 and F are the PL intensities of the plant extract without and with Au-NPs, respectively. Here, $[Q]$ represents the concentration of the quenching agent, and K_{SV} is the Stern-Volmer constant. Insert of Figure 6 displays the Stern-Volmer plot, which yields a K_{SV} value of $7.72 \times 10^3 \text{ M}^{-1}$. According to the report in the article [17], the linearity of the Stern-Volmer plot indicates a dynamic quenching mechanism.

3.4. XRD pattern analysis.

X-ray diffraction is a non-destructive technique that provides researchers and scientists with valuable information on crystal phase, lattice type, lattice constants, crystallite size, material strain, and more. Figure 7 shows the XRD patterns of (a) the plant extract and (b) Au nanofluids containing 18.72 mM Au NPs synthesized with the plant extract. The sharp peaks observed for Au NPs at Bragg diffraction angles $2\theta = 38.120^\circ$, 44.490° , and 64.50° were matched to the Miller indices (111), (200), and (220), respectively, which are consistent with the standard powder diffraction data for gold (JCPDS 00–001-1172) [12]. Bi *et al.* [18] reported seven distinct diffraction peaks between 30° and 85° , corresponding to various lattice planes such as (111), (200), (220), (311), and others, suggesting a face-centered cubic (fcc) lattice for

the Au NPs. According to the extinction rule, the lattice type is face-centered cubic (*fcc*) as the *h*, *k*, and *l* values are either all even or all odd. The intense XRD peak at $2\theta = 38.120^\circ$ indicates that most Au NPs are oriented in the (111) plane of the *fcc* lattice [12].

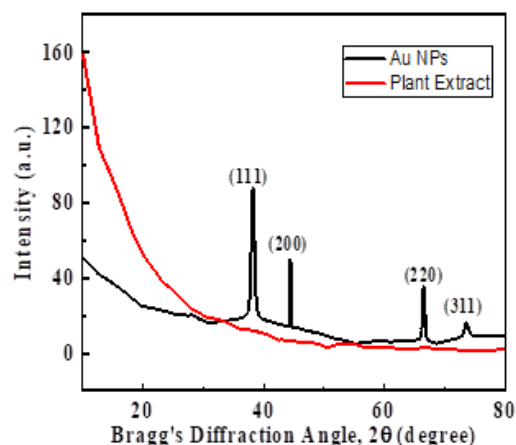


Figure 7. XRD pattern of plant extract and 10.08 mM Au NPs.

The average crystallite size, calculated from the intense (111) peak using the Debye-Scherrer equation, was determined to be 40 nm. Dong *et al.* [19] reported an average crystallite size of 50 nm for Au NPs synthesized using mulberry leaf extract.

3.5. FE-SEM and TEM micrographs.

Scanning electron micrographs serve as a potent instrument utilized by researchers across diverse domains, including materials science, biology, geology, and electronics. It aids in gathering insights on surface topography, particle size and distribution, microstructure, and more derived from micrographs of NPs. The micrographs presented in Figure 8 display three samples with varying Au contents. As evident from the image-A, in the sample containing 4 mM Au NPs, the Au clusters exhibit nearly spherical shapes and monodisperse with sizes ranging between 20 and 50 nm, whereas in the sample with 18.72 mM NPs, the size ranges between 100-120 nm. Moreover, it is observed that the cluster size increases with higher Au contents, which could be attributed to a reduction in the number of capping molecules per Au cluster. Bidan *et al.* [12] reported quasi-spherical Au nanoparticles (NPs) with sizes ranging from 30 to 50 nm, synthesized using *Jasminum sambac* (*L.*) flower extract. Muniyappan *et al.* [3] reported well-dispersed Au nanoparticles (NPs) stabilized with *Curcuma pseudomontana*, having an average size of 39 nm.

Further image analysis was conducted using a Transmission Electron Microscope (TEM), which offers higher resolution than FE-SEM. A high-quality TEM image yields information such as the sample's nanoscale morphology, crystal structure, interplanar spacing, crystal orientation, grain boundaries, crystal defects, particle size, and distribution. To enable a comprehensive microscopic comparison, TEM images were captured for the three samples previously examined by FE-SEM. The TEM images also reveal nearly spherical particles, consistent with observations from the FE-SEM images. The TEM images (Figure 9) revealed an average cluster size ranging between 20-120 nm. For the sample containing 4.72 mM Au nanoparticles (NPs), the size ranges between 20 and 50 nm, as observed in imageA of Figure 9. Consistent with observations from the FE-SEM analysis, an increase in the Au contents correlated with an increase in cluster size. Interplanar spacing (*d*-spacing) was determined from a highly resolved image (see inset of Figure 7), yielding a value of 0.235 nm, corresponding to

the Miller indices (111) of the face-centered cubic (fcc) gold lattice. A value of d-spacing 0.235 is also reported for Poly(vinyl alcohol) stabilized Au NPs [21]. Poly(vinyl pyrrolidone) assisted Au NPs give a d-spacing of 0.233 nm [17].

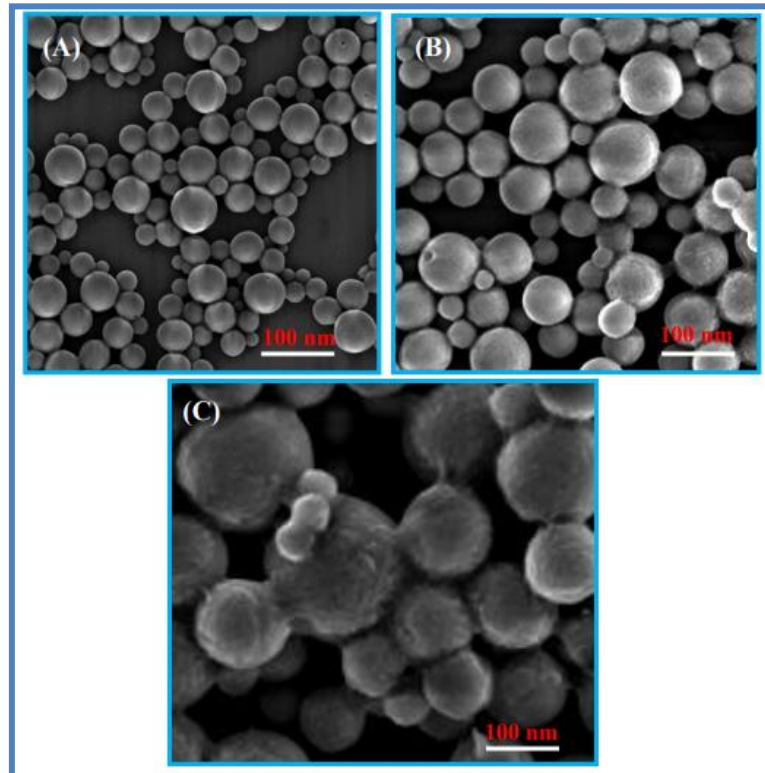


Figure 8. SEM micrographs of (A) 4.32;(B) 10.08;(C) 19.72 mM Au NPs.

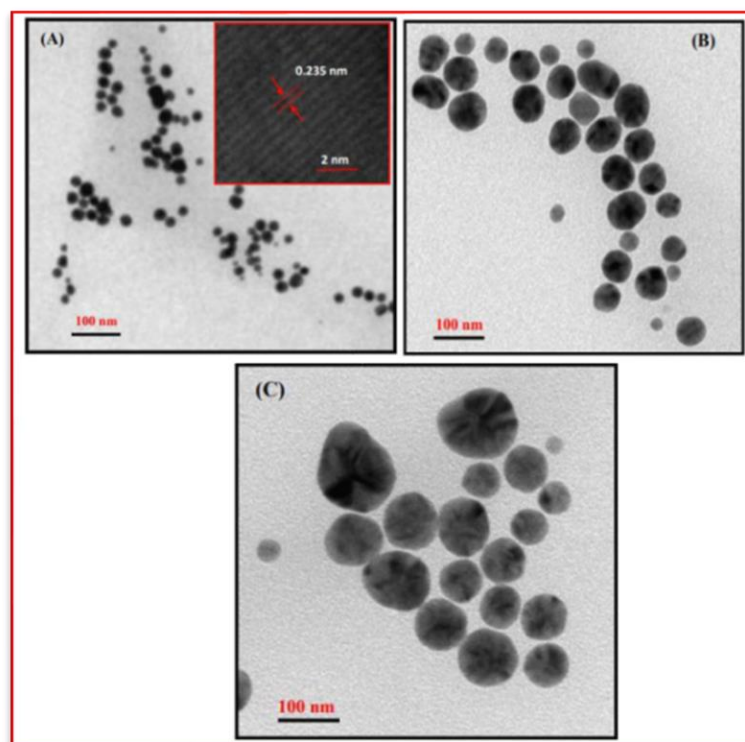


Figure 9. TEM micrographs of (A) 4.32;(B) 10.08;(C) 19.72 mM Au NPs.

Au nanoparticles (NPs) synthesized using *Saussureaobvallata* plant extract and microwave irradiation were nearly spherical, with an average size of 13 nm [20]. Peng *et al.*

[22] reported that the nanoparticles synthesized using *Acorus calamus* leaf extract were nearly spherical in shape, with sizes ranging between 30 and 50 nm.

3.6. Hydrodynamic diameter and zeta-potential.

We utilized dynamic light scattering (DLS), a non-destructive technique, to determine the hydrodynamic size, clustering behavior, polydispersity index, and zeta potential of the plant extract and five synthesized Au nanofluids in an aqueous medium. Figure 10 presents the DLS spectra of (a) the plant extract and Au nanofluids containing (b) 80 mM, (c) 100 mM, and (d) 250 mM Au nanoparticles.

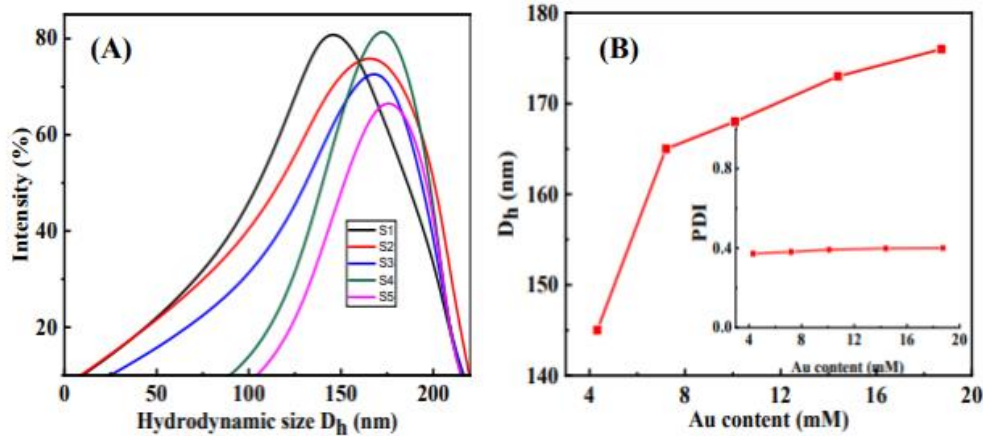


Figure 10. (A) Variation of DLS band with D_h of Au nanofluids: (a) 0, (b) 4.32; (c) 10.08; (d) 14.4; and (e) 18.72 mM Au NPs; (B) Variation of D_h with Au content (insert shows the variation of PDI with Au content).

Table 1 provides information such as average hydrodynamic diameter (D_h), polydispersity index (PDI), zeta-potential for the plant extract, and Au nanofluids. Figure 10 shows that each sample exhibited a single DLS band and exhibited monodispersity. This monodispersity is attributed to the adequate stabilizing effect of the molecules present in the plant extract.

Table 1. Average hydrodynamic diameter, Polydispersity index, and Zeta potential values of plant extract and gold nanofluids of different concentrations.

Samples	Average D_h (nm)	PDI	Zeta potential (mV)
Plant Extract	20	0.361	-9.57
Au Nanofluids (4.32mM AuNPs)	145	0.372	-14.7
Au Nanofluids (10.08 mM AuNPs)	168	0.392	-13.5
Au Nanofluids (14.4 mM AuNPs)	173	0.398	-13.0
Au Nanofluids (18.72 mM AuNPs)	176	0.400	-12.0

The variation of the average hydrodynamic diameter (D_h) with Au content is depicted in Figure 10B. The D_h value is highest for the nanofluids containing 18.72 mM Au nanoparticles. The high D_h value is attributed to the insufficient availability of plant molecules to prevent the clustering tendency of Au atoms. The article [23] reports that an increased relative number of capping molecules per nanoparticle leads to the formation of particles with a relatively smaller hydrodynamic diameter. A non-linear relationship is observed between size and Au content. The non-linear relationship between D_h and Au content is due to various

factors, such as the viscosity of the medium, the concentration of nanoparticles, and the dielectric constant of the medium. As shown in the insert of Figure 10b, the polydispersity index (PDI) of all the gold (Au) nanofluids remains nearly constant, regardless of the concentration of Au nanoparticles (NPs).

The zeta potential values obtained for the plant extract and Au nanofluids were studied to understand the nature of the surface charge (positive/negative) present on the Au NPs, the stability of the hydrocolloids, the tendency to aggregate, the type of interaction among the Au NPs in the liquid medium, and the type of dispersion. Figure 11 shows the distribution of zeta potential in the plant extract and Au nanofluids. All the samples in an aqueous medium exhibit a single zeta band, indicating electrostatic interaction between the nanoparticles, as all samples have an average negative zeta potential of -13.3 mV. The colloidal stability of the Au nanofluids is due to interparticle repulsion between the negatively charged Au nanoparticles in a high dielectric constant medium. Gold nanoparticles developed using marine microalgae have a zeta potential of -21.5 mV [7], whereas Bidan *et al.* [12] reported a surface charge of -9.37 mV for Au nanoparticles synthesized using biomolecules.

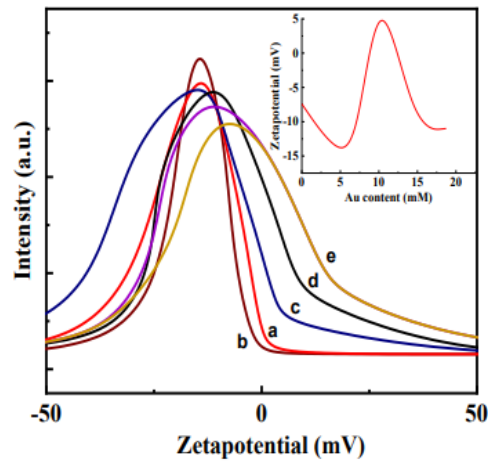


Figure 11. Zeta band distribution of Au Nanofluids with (a) 0, (b) 4.32; (c) 7.2; (d) 10.08; (e) 14.4; and (f) 18.72 mM Au NPs (insert shows the variation of zeta-potential with Au content).

3.7. Antibacterial activity study.

We studied the antibacterial activity of our bio-synthesized Au nanofluids against both gram-positive (*Bacillus subtilis*) and gram-negative (*Escherichia coli* and *Pseudomonas aeruginosa*) bacteria using the widely used Kerby-Bauer method. Azithromycin, a commercially available antibiotic, was taken as control. It is reported that the antibacterial activity of NPs depends on various factors like size and shape of NPs, roughness, dispersivity, surface charge, temperature of the medium, pH, and osmotic pressure[11, 24-27].

Table 2. Zone of inhibition shown by gold nanofluids against different bacteria

Microorganisms	P (Plant extract)	(a)S1 (4.32 mM)	(b)S2 (7.2 mM)	(c)S3 (10.08 mM)	(d)S4 (14.72 mM)	(e)S5 (18.72 mM)	AZM (Azithromycin)
<i>Bacillus subtilis</i>	-	-	4 mm	6 mm	6 mm	6 mm	9 mm
<i>Escherichia coli</i>	-	-	-	6 mm	7 mm	7 mm	20 mm
<i>Pseudomonas aeruginosa</i>	-	-	4 mm	6 mm	8 mm	8 mm	17 mm

Figures 12, 13, and 14 and Table 2 show the zone of inhibition study against the three selective bacteria. Insignificant zones of inhibition were seen around the wells, as observed in Figure 12-14.

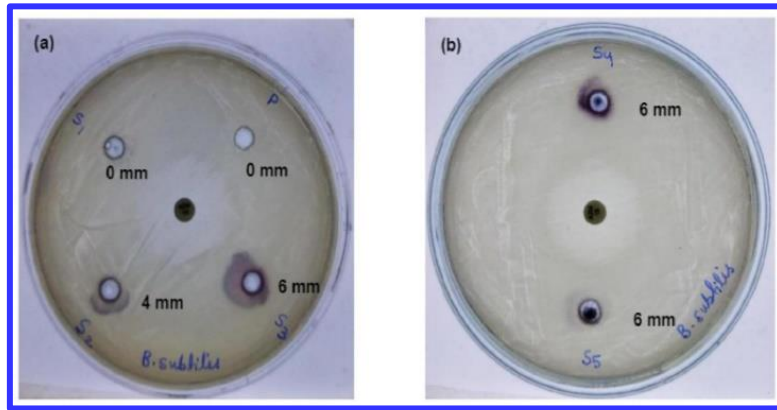


Figure 12. Antibacterial activity test against *Bacillus subtilis*.

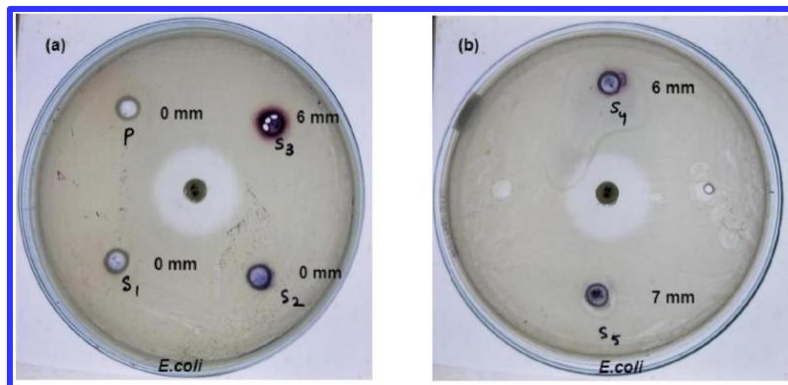


Figure 13. Antibacterial activity test against *Escherichia coli*.

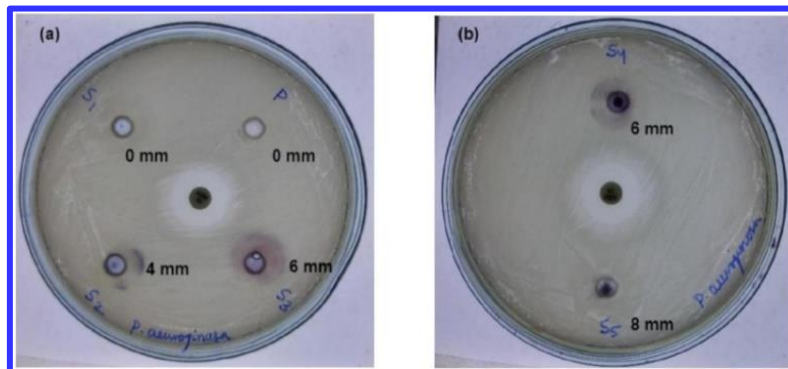


Figure 14. Antibacterial activity test against *Pseudomonas aeruginosa*.

This suggests that the nanoparticle sizes are too large to penetrate the bacterial cell wall or plasma membrane, preventing them from lysing the bacteria [24]. The bacterial cell walls carry an electrostatic negative charge, and our zeta potential study indicates that gold nanoparticles also have a negative charge, likely causing electrostatic repulsion between the gold nanoparticles and the bacterial cell wall [25,26]. Our findings indicate that gold nanoparticles in an aqueous medium may be effective at killing bacteria, particularly in *Plumeria Pudica* leaf extract [27]. *Plumeria pudica* leaves extract alone did not show antimicrobial activity. Further investigation is needed to find the reason for the nanofluids' low antibacterial activity and the leaf extract's antimicrobial activity.

4. Conclusions

Gold nanoparticles were synthesized using *Plumeria pudica* leaf extract in an aqueous medium, resulting in nearly spherical Au NPs. The absorption spectrum shows a decrease in the intensity of the $\pi \rightarrow \pi^*$ band at 324 nm of plant molecules, indicating a donor-acceptor type interaction between Au NPs and the plant molecules. A shift in the carbonyl band ($>C=O$) of plant molecules suggests their interaction with Au NPs. The emission band intensity of plant molecules decreases in the presence of Au NPs, following a dynamic quenching mechanism as shown by a Stern-Volmer plot. Both FESEM and TEM micrographs confirm the formation of nearly spherical Au NPs in the nanofluids. Zeta-potential measurements indicate that the metallic surface of the Au NPs is negatively charged. The synthesized Au nanofluids exhibited small antibacterial activity against *Bacillus subtilis*, *Escherichia coli*, and *Pseudomonas aeruginosa*. Further investigation is needed to understand why the Au nanofluids were not very effective in inhibiting the growth of bacteria. Possible reasons could include the need for different concentrations of nanoparticles, surface modifications of nanoparticles, or interactions with the bacterial cell walls.

Funding

This research received no external funding

Acknowledgments

We greatly acknowledge the support from Silicon University, Odisha, and Trident Academy of Creative Technology, Bhubaneswar.

Conflicts of Interest

There are no conflicts to declare.

References

1. Vijayakumar, S. Eco-friendly synthesis of gold nanoparticles using fruit extracts and *in vitro* anticancer studies. *J. Saudi Chem. Soc.* **2019**, *23*, 753-761, <https://doi.org/10.1016/j.jscs.2018.12.002>.
2. Li, S.; Al-Misned, F.A.; El-Serehy, H.A.; Yang, L. Green synthesis of gold nanoparticles using aqueous extract of *Mentha Longifolia* leaf and investigation of its anti-human breast carcinoma properties in the *in vitro* condition. *Arab. J. Chem.* **2021**, *14*, 102931, <https://doi.org/10.1016/j.arabjc.2020.102931>.
3. Muniyappan, N.; Pandeewaran, M.; Amalraj, A. Green synthesis of gold nanoparticles using *Curcuma pseudomontana* isolated curcumin: Its characterization, antimicrobial, antioxidant and anti-inflammatory activities. *Environ. Chem. Ecotoxicol.* **2021**, *3*, 117-124, <http://dx.doi.org/10.1016/j.enceco.2021.01.002>.
4. Thipe, V.C.; Karikachery, A.R.; Çakılkaya, P.; Farooq, U.; Genedy, H.H.; Kaeokhamloed, N.; Phan, D.-H.; Rezwani, R.; Tezcan, G.; Roger, E.; Katti, K.V. Green nanotechnology—An innovative pathway towards biocompatible and medically relevant gold nanoparticles. *J. Drug Deliv. Sci. Technol.* **2022**, *70*, 103256, <https://doi.org/10.1016/j.jddst.2022.103256>.
5. Khan, N.; Durrani, P.; Jamila, N.; Nishan, U.; Jan, M.I.; Ullah, R.; Bari, A.; Choi, J.Y. *Hymenaea courbaril* resin-mediated gold nanoparticles as catalysts in organic dyes degradation and sensors in pharmaceutical pollutants. *Heliyon* **2024**, *10*, e30105, <https://doi.org/10.1016/j.heliyon.2024.e30105>.
6. De Matteis, V.; Cascione, M.; Pellegrino, P.; Di Corato, R.; Catalano, M.; Miraglia, A.; Scarano, A.; Santino, A.; Chieppa, M.; Rinaldi, R. Multishaped bio-gold polyphenols bearing nanoparticles to promote inflammatory suppression. *Nano Today* **2024**, *57*, 102329, <https://doi.org/10.1016/j.nantod.2024.102329>.
7. Rosyidah, A.I.; Purbani, D.C.; Pratiwi, R.D.; Muttaqien, S.E.; Nantapong, N.; Warsito, M.F.; Fikri, M.N.; Ruth, F.; Gustini, N.; Syahputra, G.; Padri, M.; Noerdjito, D.R.; Nurkanto, A.; Afani, H. Eco-friendly

- synthesis of gold nanoparticles by marine microalgae *Synechococcus moorigangae*: Characterization, antimicrobial, and antioxidant properties. *Kuwait J. Sci.* **2024**, *51*, 100194, <https://doi.org/10.1016/j.kjs.2024.100194>.
8. Vorobyova, V.; Skiba, M.; Khrokalo, L.; Vasyliiev, G. Exploring the Potential of DES III Type for Grape Pomace Extraction, Phytochemical Synthesis of Gold Nanoparticles and Evaluating Cytotoxicity and Antibacterial Properties. *Chem. Afr.* **2024**, *7*, 2253-2264, <https://doi.org/10.1007/s42250-024-00877-7>.
 9. Adamu, H.I.; Faruruwa, M.D.; Adeyemi, M.M.; Tomori, W.B.; Akorede, A.O. Plant Synthesized Iron Oxide Nanoparticles for Removal of Emerging Contaminant. *Chem. Afr.* **2024**, *7*, 1173-1186, <https://doi.org/10.1007/s42250-023-00822-0>.
 10. Serdar, G. Biosynthesis and Characterization of Gold Nanoparticles Using Microwave-Assisted Technology from Pomegranate (*Punica granatum* L.) Leaf Extract Produced by the Method of Supercritical Fluid Extraction (SFE). *Plasmonics* **2024**, *19*, 2233-2243, <https://doi.org/10.1007/s11468-024-02312-6>.
 11. Ogwuche, C.E.; Elemike, E.E.; Oju, D.; Onwudiwe, D.C.; Singh, M.; Akpeji, B.H. Synthesis, Characterization, Anticancer and Antimicrobial Potentials of *Chrysothemis Pulchella* Leaf Extract Mediated Gold Nanoparticles. *J. Inorg. Organomet. Polym. Mater.* **2024**, *34*, 944-951, <https://doi.org/10.1007/s10904-023-02817-3>.
 12. Bidan, A.K.; Al-Ali, Z.S.A. Assessment of Defeating of Breast Cancer MCF-7 Cells, and Bacterial Species by Spherical Gold Nanoparticles Fabricated Through Reductive Ability of Framed Bio-Organic Molecules. *Chem. Afr.* **2024**, *7*, 3789-3808, <https://doi.org/10.1007/s42250-024-00979-2>.
 13. Melo, A.A.; Rodrigues, E.P.; Vasconcelos, J.S.; Medeiros, E.S.; Oliveira, L.C.; Lima, A.M.N. Dielectric Function of Gold Nanoparticles Synthesized Using *Camellia sinensis* Extract. *Plasmonics* **2023**, *18*, 529-540, <https://doi.org/10.1007/s11468-022-01776-8>.
 14. Mary Mawumenyo Mamattah, K.; Kusiwaa Adomako, A.; Nketia Mensah, C.; Borquaye, L.S. Chemical Characterization, Antioxidant, Antimicrobial, and Antibiofilm Activities of Essential Oils of *Plumeria alba* (Forget-Me-Not). *Biochem. Res. Int.* **2023**, *2023*, 1040478, <https://doi.org/10.1155/2023/1040478>.
 15. Tripathy, A.; Behera, M.; Rout, A.S.; Biswal, S.K.; Phule, A.D. Optical, Structural, and Antimicrobial Study of Gold nanoparticles Synthesized Using an Aqueous Extract of *Mimusops elengi* Raw Fruits. *Biointerface Res. Appl. Chem* **2020**, *10*, 7085-7096, <https://doi.org/10.33263/BRIAC106.70857096>.
 16. Behera, M.; Ram, S. Spectroscopy-based study on the interaction between gold nanoparticle and poly(vinylpyrrolidone) molecules in a non-hydrocolloid. *Int. Nano Lett.* **2013**, *3*, 17, <https://doi.org/10.1186/2228-5326-3-17>.
 17. Behera, M.; Ram, S. Intense quenching of fluorescence intensity of poly(vinyl pyrrolidone) molecules in the presence of gold nanoparticles. *Appl. Nanosci.* **2013**, *3*, 543-548, <https://doi.org/10.1007/s13204-012-0159-8>.
 18. Bi, M.; Li, Y.; Lv, F.; Shi, W.; Jiang, G. The Attenuating Effect of Curcumin-Loaded Gold Nanoparticles and Its Combination with *Pluchea indica* Root Extract on Kidney Stone Induced Male Wistar Rats. *J. Clust. Sci.* **2024**, *35*, 327-340, <https://doi.org/10.1007/s10876-023-02483-y>.
 19. Dong, C.; Fu, R.; Yu, S.; Guo, X.; Chen, W. Biosynthesis and Characterization of Monodisperse Gold Nanoparticles using Mulberry Leaf Extract at Room Temperature. *Russ. J. Phys. Chem. B* **2024**, *18*, 599-606, <https://doi.org/10.1134/S1990793124020064>.
 20. Dalavi, P.A.; V, A.J.; Thomas, S.; Prabhu, A.; Anil, S.; Seong, G.H.; Venkatesan, J. Microwave-Assisted Biosynthesized Gold Nanoparticles Using *Saussurea obvallata*: Biocompatibility and Antioxidant Activity Assessment. *BioNanoSci.* **2022**, *12*, 741-751, <https://doi.org/10.1007/s12668-022-00994-y>.
 21. Behera, M. An intensive study on the optical, rheological, and electrokinetic properties of polyvinyl alcohol-capped nanogold. *Int. Nano Lett.* **2015**, *5*, 161-169, <https://doi.org/10.1007/s40089-015-0150-y>.
 22. Peng, H.; Zhang, S.; Chai, Q.; Hua, Z. Green synthesis of gold nanoparticles using *Acorus calamus* leaf extract and study on their anti-alzheimer potential. *Biotechnol. Bioprocess Eng.* **2024**, *29*, 157-163, <https://doi.org/10.1007/s12257-024-00010-y>.
 23. Behera, M.; Ram, S. Solubilization and stabilization of fullerene C₆₀ in the presence of poly(vinyl pyrrolidone) molecules in water. *J. Incl. Phenom. Macrocycl. Chem.* **2012**, *72*, 233-239, <https://doi.org/10.1007/s10847-011-9957-y>.
 24. Jiang, Y.; Zheng, W.; Tran, K.; Kamilar, E.; Bariwal, J.; Ma, H.; Liang, H. Hydrophilic nanoparticles that kill bacteria while sparing mammalian cells reveal the antibiotic role of nanostructures. *Nat. Commun.* **2022**, *13*, 197, <https://doi.org/10.1038/s41467-021-27193-9>.

25. Wilhelm, M.J.; Sharifian Gh, M.; Wu, T.; Li, Y.; Chang, C.-M.; Ma, J.; Dai, H.-L. Determination of bacterial surface charge density via saturation of adsorbed ions. *Biophys. J.* **2021**, *120*, 2461-2470, <https://doi.org/10.1016/j.bpj.2021.04.018>.
26. Joshi, A.S.; Singh, P.; Mijakovic, I. Interactions of Gold and Silver Nanoparticles with Bacterial Biofilms: Molecular Interactions behind Inhibition and Resistance. *Int. J. Mol. Sci.* **2020**, *21*, 7658, <https://doi.org/10.3390/ijms21207658>.
27. Vo, T.-T.; Nguyen, T.T.-N.; Huynh, T.T.-T.; Vo, T.T.-T.; Nguyen, T.T.-N.; Nguyen, D.-T.; Dang, V.-S.; Dang, C.-H.; Nguyen, T.-D. Biosynthesis of Silver and Gold Nanoparticles Using Aqueous Extract from *Crinum latifolium* Leaf and Their Applications Forward Antibacterial Effect and Wastewater Treatment. *J. Nanomater.* **2019**, *2019*, 8385935, <https://doi.org/10.1155/2019/8385935>.